CAV2021
11th International Symposium on Cavitation
May 10-13, 2021, Daejon, Korea

LES of cavitating shear layer

Filipe Brandao [1], Krishnan Mahesh [1*]

[1]Department of Aerospace Engineering and Mechanics, University of Minnesota, Minneapolis, MN, USA

Abstract: Shear layer cavitation is numerically investigated at inception conditions in a backward-facing step configuration. A turbulent boundary layer is used as the inflow boundary conditions to match experiments where mean and root-mean-square values of velocity at the shear layer are validated with experimental data. We use a novel methodology that treats vapor as a passive scalar in an incompressible liquid. We show that inception occurs inside the core of the streamwise stretched/contracted vortical structures along the shear layer in axial positions around 67% of the reattachment point, which is in good agreement with experiments.

Keywords: inception; shear layer; turbulent boundary layer

1. Introduction

Cavitation is the name given to the process of vapor formation due to a drop in pressure. This phenomenon can occur at different scales depending on the ambient pressure, from inception to a more developed state. In some cases where multiple vortices interact, like turbulent shear layers and wakes of marine geometries, inception can be observed in the weaker vortices for a relatively higher ambient pressure [1,2]. Therefore, mechanisms that lead to cavitation inception in such cases are of interest. The inception regime is hard to predict both numerically and experimentally. Experimentally, inception can be determined through visual and acoustical techniques when the measurements detect events per unit time above a certain threshold [3]. Numerically, the most used approach employs an Euler-Lagrange framework. There, the liquid follows the incompressible Navier-Stokes equations while each bubble is tracked individually with the equations of motion coupled with Rayleigh-Plesset equation for their size [4,5]. Another approach is based on the compressible homogenous mixture model where liquid and vapor are considered a single medium with thermal and mechanical equilibrium between phases [6,7]. This approach, however, is expensive in the inception regime due to the small timesteps required. In the present paper we use a new method to simulate inception based on passive scalar, as briefly described in [8], to investigate inception in turbulent shear layer of a backward-facing step at $Re_\tau = 1500$ and at the cavitation number of $\sigma = 0.55$.

2. Governing equation and numerical method

In the present work, we perform large-eddy simulation (LES) of cavitation inception by treating vapor as a passive scalar in an incompressible liquid. The main idea behind is that since inception is a stochastic process that generates small amounts of vapor for short periods of time, the effects of these small regions of vapor on the liquid density and flow dynamics can be negligible. We, therefore, solve the incompressible Navier-Stokes equation for the liquid while an advection-diffusion equation with source terms is solved for the vapor concentration. The filtered equations are given by

* Corresponding Author: Krishnan Mahesh, kmahesh@umn.edu

$$\frac{\partial \overline{u_i}}{\partial x_i} = 0,$$
$$\frac{\partial \overline{u_i}}{\partial t} + \frac{\partial \overline{u_i}\,\overline{u_j}}{\partial x_j} = -\frac{\partial \bar{p}}{\partial x_i} + \nu \frac{\partial^2 \overline{u_i}}{\partial {x_j}^2} - \frac{\partial \tau_{ij}}{\partial x_j}, \tag{1}$$
$$\frac{\partial \bar{C}}{\partial t} + \frac{\partial \bar{C}\overline{u_j}}{\partial x_j} - \frac{\nu}{Sc}\frac{\partial^2 \bar{C}}{\partial {x_j}^2} + \frac{\partial \tau_C}{\partial x_j} = S_e - S_c.$$

Here, the passive scalar is taken as the vapor concentration, $C = \rho_v \alpha$ where α is the vapor volume fraction and $\rho_v = 0.749\ kg/m^3$ is the vapor density. The subgrid scale stress is given by $\tau_{ij} = \overline{u_i u_j} - \overline{u_i}\,\overline{u_j}$ while the subgrid scalar flux is given by $\tau_C = \overline{C u_j} - \bar{C}\overline{u_j}$. They are computed using the dynamic Smagorinsky eddy viscosity model [9] and eddy diffusivity model [10], respectively. The cavitation source term is given by Saito *et al.* [11] and the Schmidt number for vapor in water is $Sc = 500$.

It can be noted that the diffusion term for the advection-diffusion equation is very small. This results in the absence of dissipation, which becomes problematic for regions with large gradients of the scalar field. To avoid using very small timesteps to solve both Navier-Stokes and the advection-diffusion equations, we use the approach proposed in Muppidi and Mahesh [12] where the scalar field is advanced in time with a smaller timestep than the one used for the velocity field in an inner loop.

3. Results

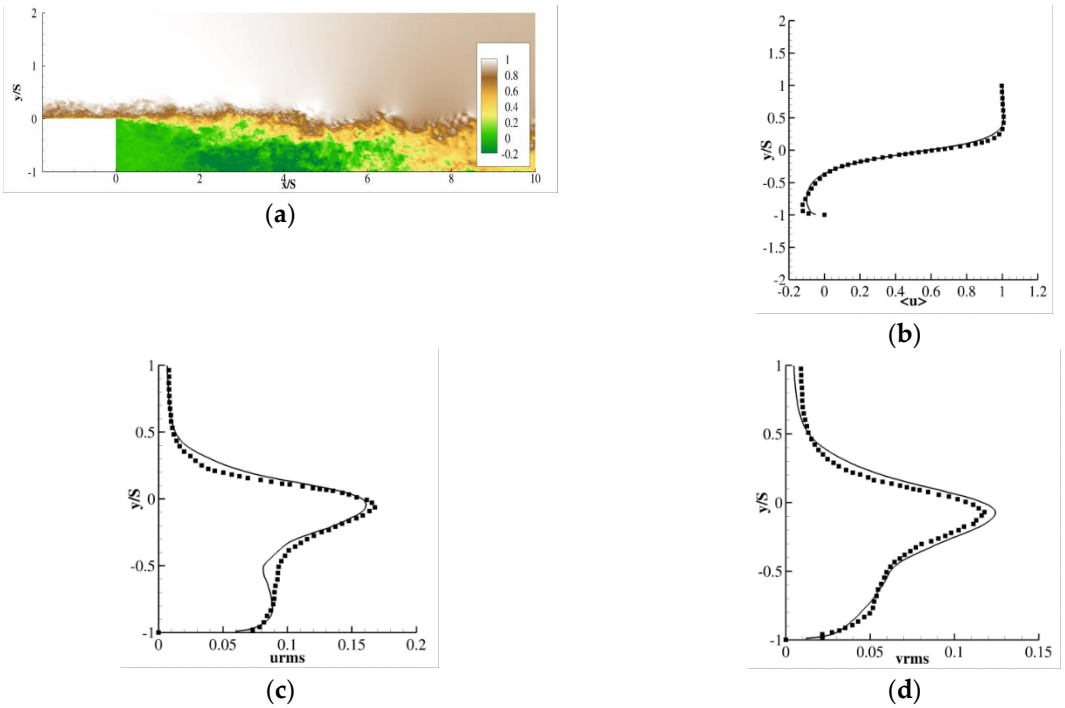

(**a**) (**b**) (**c**) (**d**)

Figure 1. Instantaneous contours of velocity at the domain center plane (**a**). Comparison of mean velocity profile and profiles of $\sqrt{u'^2}$, $\sqrt{v'^2}$ with [13] are given in (**b**), (**c**) and (**d**) respectively at $x = 2S$. Lines: numerical results. Symbols: experimental results.

* Corresponding Author: Krishnan Mahesh, kmahesh@umn.edu

Shear layer inception is investigated in the backward-facing step configuration of Agarwal *et al.* [13]. The grid used has approximately 190 million control volumes with resolution near the step of $\Delta x^+ = 12$, $\Delta y^+ = 0.61$ and $\Delta z^+ = 32$. A vapor concentration equivalent to a volume fraction of $\alpha = 1 * 10^{-5}$ is prescribed in the inflow. A velocity field of a turbulent boundary-layer at $Re_\tau = 1500$ is used as inflow boundary condition to match experiments. Figure 1 shows velocity profiles at a location $x = 2S$ downstream of the step (S) and velocity contours at the center plane. The flow separation at the step corner and the formation of a recirculating region can be observed. The numerical results show good agreement with experimental data of [13]. The reattachment length (L_r) is predicted to be around $L_r = 6S$, overpredicting the experimental value of $L_r = 5.5S$

Figure 2 shows probability density function (PDF) of pressure and vapor volume fraction between $x = 3S$ ($0.5L_r$) and $x = 6S$ (L_r). The PDFs reveal that the probability of finding low pressure events in this region decreases with axial distance. The probability of finding regions of vapor seems confined around $x = 4S$ ($0.67L_r$), which is in good agreement with the experimental range observed in Agarwal *et al.* [13]. It is also interesting to observe that the locations with higher probability of low pressure events do not necessarily match with the locations with higher probability of finding vapor. The stations of $x = 3S$ and $x = 4S$, for example, show similar PDF curves for pressure, but the PDF curves for volume fraction are orders of magnitude apart. This indicates the effects of finite rate evaporation and condensation. Low pressure regions need to be sustained for some amount of time to allow for the growth of vapor to more visible sizes. Figure 2 (a) and (b) show that, for $\sigma = 0.55$, the cavitation process starts at $x = 3S$ and the vapor grows slowly as it is advected following the low pressure regions to $x = 4S$. As the vapor is advected further to $x = 5S$, it is condensed back to freestream levels due to pressure recover as shown by the PDF curves.

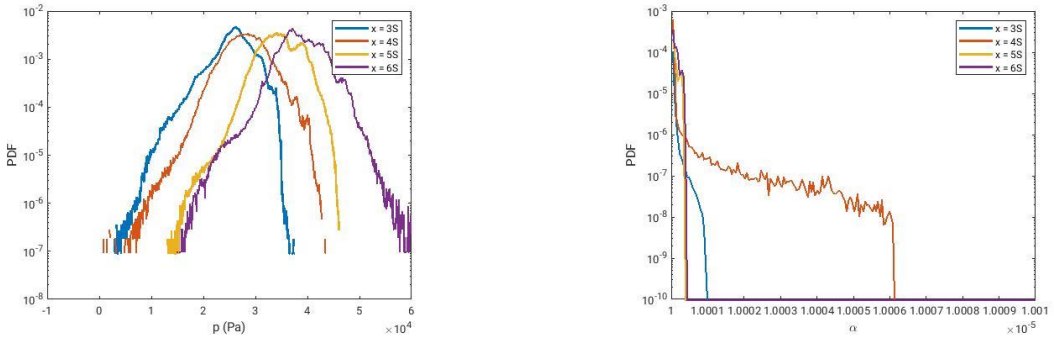

(**a**) (**b**)

Figure 2. PDF of pressure (**a**) and vapor volume fraction (**b**) for $\sigma = 0.55$.

O'Hern [1] found that inception would primarily occur in the stretched streamwise vortices, indicating that the lowest values of pressure are likely to be in the core of these vortices. The invariants of the velocity gradient tensor as well as of the strain rate tensor and rotation rate tensor help identify the flow structures that contain pressure minima. Figure 3 (a) shows joint-PDF between the second (Q) and third (R) invariants of the velocity gradient tensor. Regions of the flow lying above the solid black line indicate that fluid particles are undergoing stretching ($R < 0$) or contraction ($R > 0$). Figure 3 (b) shows joint-PDF between the second invariants of the strain rate tensor (Qs) and the rotation rate tensor (Qw). Regions of the flow lying below the solid black line are dominated by rotation (such as a vortex core) while regions lying above the line are dominated by strain (such as the more outside regions of a vortex). For more details, the reader is referred to [14]. All the points collected for figure 3 are regions where the local pressure is lower than the vapor pressure.

* Corresponding Author: Krishnan Mahesh, kmahesh@umn.edu

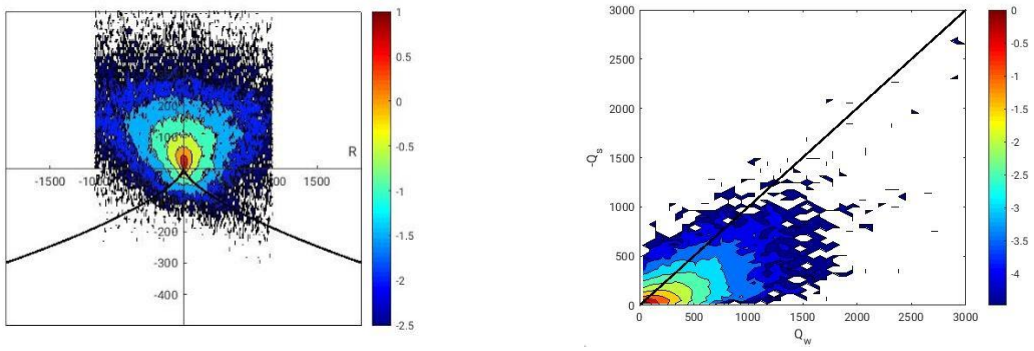

Figure 3. Joint-PDFs of $Q - R$ (**a**) and $Qs - Qw$ (**b**). Levels in both plots are in logarithmic scale.

The joint-PDF of $Q - R$ in figure 3 (a) reveals that pressure drops below vapor pressure primarily in regions where the flow is being either stretched or contracted. The joint-PDF in figure 3 (b) shows that these events are likely to be dominated by rotation. This confirms the conclusion predicted by O'Hern [1] that the pressure minima and cavitation inception occur inside the core of vortices that are being stretched or contracted. Figure 4 shows an example of these structures. Isocontour of $p = p_v$ is given in orange and isocontour of $\alpha = 1.005 * 10^{-5}$ is given in blue. It can be observed the presence of multiple locations with pressure equal of less than vapor pressure in the shear layer, however the largest structure is the elongated streamwise vortex. The isocontour of vapor volume fraction confirms that this structure cavitates first, which agrees with experimental observations.

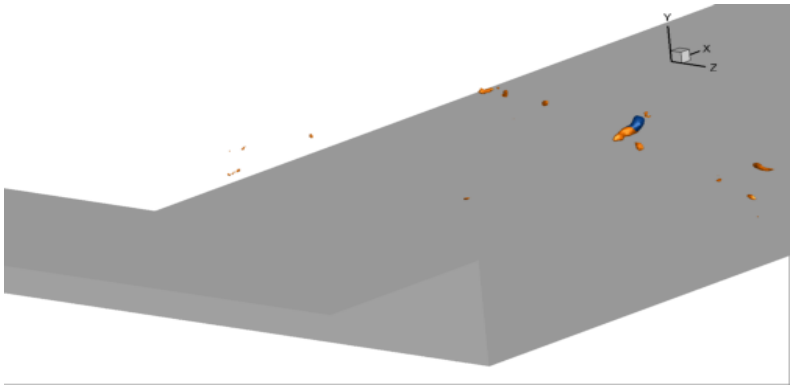

Figure 4. Isocontours of $p = p_v$ in orange and $\alpha = 1.005 * 10^{-5}$ in blue.

4. Conclusions

Cavitation inception in a shear layer was numerically investigated using the backward-facing step configuration of [13], where a novel approach that considers vapor as a passive scalar in an incompressible liquid is employed. A turbulent boundary layer at $Re_\tau = 1500$ is used as the inflow boundary condition to match experiments and good agreement is obtained for the velocity profiles. Probability density function plots show that the likelihood of low pressure events is higher between $x = 3S$ $(0.5L_r)$ and $x = 4S$ $(0.67L_r)$. It also shows that regions of vapor are more likely to be found around $x = 4S$ $(0.67L_r)$, which is within the experimental range. Joint-PDF between the invariants of velocity gradient, strain rate and rotation rate

* Corresponding Author: Krishnan Mahesh, kmahesh@umn.edu

tensors reveal that local pressure drops below vapor pressure inside the core of vortices that are being either stretched or contracted, agreeing with predictions from [1].

Acknowledgments: This work is supported by the United States Office of Naval Research under Grants ONR N00014-17-1-2676 with Dr. Ki-Han Kim as the program manager. Computing resources were provided by the High-Performance Computing Modernization Program (HPCMP). We acknowledge Karuna Agarwal and Prof. Joseph Katz at Johns Hopkins University for providing the experimental data.

References

1. O'Hern, T.J. An experimental investigation of turbulent shear flow cavitation. J. Fluid Mech. **1990**, *215*, 365-391.
2. Chang, N.A.; Choi, J.; Yakushuji, R.; Ceccio, S.L. Cavitation inception during the interaction of a pair of counter-rotating vortices. Physics of Fluids. **2012**, *24*, 1-15
3. Rood, E.P. Review – mechanisms of cavitation inception. J Fluids Eng. **1991**, *113*, 163-175.
4. Hsiao, C.T.; Chahine, G.L.; Liu, H.L. Scaling effect on prediction of cavitation inception in a line vortex flow. J. Fluids Eng. **2003**, *125*, 53-60
5. Shams, E.; Finn, J.; Apte, S.V. A numerical scheme for euler-lagrange simulation of bubbly flows in complex systems. Int. J. Numer. Meth. Fluids. **2011**, *67*, 1865-1898.
6. Gnanaskandan, A.; Mahesh, K. A numerical method to simulate turbulent cavitating flows. Int. J. of Multiphase Flows. **2015**, *70*, 22-34.
7. Brandao, F.L.; Bhatt, M.; Mahesh, K.; Numerical study of cavitation regimes in flow over a circular cylinder. J. Fluid Mech. **2020**, *885*, A19.
8. Brandao, F.L.; Madabhushi, A.; Bhatt, M.; Mahesh, K. Large eddy simulation for the investigation of different regimes of cavitation. Proceedings of the 33rd Symposium on Naval Hydrodynamics, Osaka, Japan, 2020
9. Germano, M.; Piomelli, U.; Moin, P.; Cabot, W.H. A dynamic subgrid-scaer eddy viscosity model. Physics of Fluids A. **1991**, *3(7)*, 1760-1765.
10. Moin, P.; Squires, K.; Cabot, W.; Lee, S. A dynamic subgrid-scale model for compressible turbulence and scalar transport. Physics of Fluids A. **1991**, *3(11)*, 2746-2757.
11. Saito, Y.; Takami, R.; Nakamori, I.; Ikohagi, T. Numerical analysis of unsteady behavior of cloud cavitation around NACA0015 foil. Comp. Mech. **2007**, *40*, 85-96.
12. Muppidi, S.; Mahesh, K. Direct numerical simulation of passive scalar transport in transverse jets. J. Fluid Mech. **2008**, *598*, 335-360.
13. Agarwal, K.; Ram, O.; Katz, J. Cavitating structures at inception in turbulent shear flow. Proceedings of the 10th International Symposium on Cavitation, Baltimore, USA, 2018.
14. Perry, A.E.; Chong, M.S. Topology of Flow Patterns in Vortex Motions and Turbulence. Applied Scientific Research. **1994**, *53*, 357-374.

* Corresponding Author: Krishnan Mahesh, kmahesh@umn.edu